An instrument to measure atmospheric pressure fluctuations above surface gravity waves[1]

R. L. Snyder, R. B. Long, J. Irish, D. G. Hunley, and N. C. Pflaum

Nova University
Physical Oceanographic Laboratory
8000 North Ocean Drive
Dania, Florida 33004 U.S.A.

ABSTRACT

This paper describes an instrument which has been used successfully at a field site in the Bight of Abaco, Bahamas, to monitor the atmospheric pressure field above surface gravity waves in the frequency range .5 to 5. rad/s. The atmospheric pressure is sampled at fixed elevations with a cone-shaped probe having a pressure coefficient of less than .02 magnitude for angles of attack less than 15°; the probe is mounted on a vane to minimize horizontal angles of attack. The pressure signal is conducted to a subsurface transducer through a mercury-sealed bearing. Overall system noise is estimated to be of order .5 μbars and is largely wave-incoherent.

1. Introduction

The measurement of the atmospheric pressure field associated with surface gravity waves is important to an understanding of how waves grow. This measurement, however, presents a number of difficulties which are not common to land measurement of atmospheric pressure. Because the primary interest is in the pressure field "close to" the mean surface, in particular "at" the mean surface (clearly impossible to monitor directly), the environmental conditions accompanying field observation are severe. Because it is necessary to imbed a probe in the flow, the sensitivity of the probe to dynamic pressures must be small. The latter concern is particularly troublesome in view of the wide variation in horizontal wind direction in a typical air flow above waves. Several attempts to confront these difficulties and to obtain measurements of wave-induced atmospheric pressure have been made by others; these include:

a. *Longuett-Higgins, Cartwright and Smith* (1963). A freely floating disc-shaped raft was instrumented to sample atmospheric pressure through twelve

1. Received: *26 June, 1973*; revised: *15 March, 1974*.

holes in its upper face. Special precautions were taken to keep these holes free of water. The dynamic pressure sensitivity of the instrument was not reported.

b. *Shemdin and Hsu* (1967) *and Shemdin* (1969). The atmospheric pressure above laboratory waves was monitored using a wave-following device which maintained a small disc-shaped probe (axis horizontal and perpendicular to the axis of the tunnel) .5 cm from the instantaneous water surface. The pressure coefficient for the disc-shaped probe was not reported, but it was probably in the range of .05–.10 at zero angle of attack. The probe was insensitive to fluctuations in the vertical angle of attack, and under the controlled conditions of the laboratory, fluctuations in horizontal angle of attack were presumably small.

c. *Dobson* (1971). A pressure port was located in the horizontal face of a 23-cm hinged styrofoam float riding on a vertical staff. The float was oriented into the wind by a fin. A pressure coefficient of −.04 to .02 was reported for angles of attack between ± 5° (at 6 m/s). Considerable difficulty was caused by submergence of the buoy and resultant contamination of the pressure signal.

d. *Elliot* (1972). A specially contoured, disc-shaped probe was developed with a pressure coefficient of .02 or less for angles of attack between ± 10°. This probe was used as a fixed sensor with its axis vertical. Field experiments were performed with a two-component vertical array of instruments.

The present paper describes yet another approach to the problem of monitoring the atmospheric pressure field above the water surface. This approach involves a cone-shaped probe with a pressure coefficient of .02 or less for angles of attack between ± 15°, mounted on a vane to limit horizontal angles of attack. The instrument is fixed in order to avoid inertial pressures in the system plumbing and other inertial effects, and in order to simplify the field measurements. An array of four instruments is employed to gain directional information.

2. The probe

The principal objective of the experiments for which the present instrument was developed was to monitor the wave-coherent atmospheric pressure field above waves, in order to calculate the directional cross-spectrum between surface elevation and wave-induced atmospheric pressure as related to the wind generation of waves. The primary quantity of interest was, accordingly, the covariance

$$C_{\zeta P} \equiv < \zeta(\boldsymbol{x}, t)\, P(\boldsymbol{x} + \boldsymbol{\xi}, z, t + \tau) > .$$

Of secondary interest was the covariance

$$C_{P_2} = < P(\boldsymbol{x}, z, t)\, P(\boldsymbol{x} + \boldsymbol{\xi}, z, t + \tau) > .$$

Here $\zeta(\boldsymbol{x},t)$ is the surface elevation at horizontal position $\boldsymbol{x}$ and time t, and $P(\boldsymbol{x},z,t)$ is the atmospheric pressure at horizontal position $\boldsymbol{x}$, elevation z, and time t. The brackets denote an ensemble average.

The pressure Q measured by a static pressure probe typically contains a fraction μ of the dynamic pressure,

$$Q = P + \frac{1}{2}\mu\varrho|\boldsymbol{W}|^2.$$

ϱ is the density of air. The pressure coefficient μ is a function of the orientation of the probe relative to the horizontal wind velocity $\boldsymbol{W}$. This orientation, the pressure coefficient μ, the static pressure P, and the wind velocity $\boldsymbol{W}$ are all random functions of space and time expressible in the form

$$\mu = \mu_0 + \mu_1 + \mu_1' + \ldots,$$

$$\boldsymbol{W} = \boldsymbol{W}_0 + \boldsymbol{W}_1 + \boldsymbol{W}_1' + \ldots,$$

and

$$P = P_0 + P_1 + P_1' + \ldots,$$

where the first-order fields consist of a wave-coherent (unprimed) and a wave-incoherent or turbulent (primed) field. To second order,

$$C_{\zeta Q} = C_{\zeta_1 P_1} + \varrho\mu_0 \boldsymbol{W}_0 \cdot \boldsymbol{C}_{\zeta_1 \boldsymbol{W}_1} + \frac{1}{2}\varrho W_0^2 C_{\zeta_1 \mu_1} + \ldots, \tag{1}$$

since, by definition, covariances such as $C_{\zeta_1 P_1'}$ vanish.

Similarly,

$$C_{Q^2} = C_{P_1^2} + C_{P_1'^2} + \text{terms in } \mu_0, \mu_1, \text{and } \mu_1'. \tag{2}$$

The second and third terms on the right-hand side of equation (1) and the terms in μ_0, μ_1, and μ_1' of equation (2) represent errors resulting from the dynamic pressure sensitivity of the system. These errors may be made to vanish by designing the probe and probe installation so that $\mu_0 = 0$, $\mu_1 = 0$, and $\mu_1' = 0$. Let χ and ψ be the horizontal and vertical angles of attack, respectively. Then, expanding in Taylor series,

$$\mu = \mu(\chi,\psi) = \mu(0,0) + \chi\frac{d}{d\chi}\mu(0,0) + \psi\frac{d}{d\psi}\mu(0,0) + \ldots.$$

But

$$\chi = \chi_1 + \chi_1' + \ldots,$$

and

$$\psi = \psi_1 + \psi_1' + \ldots.$$

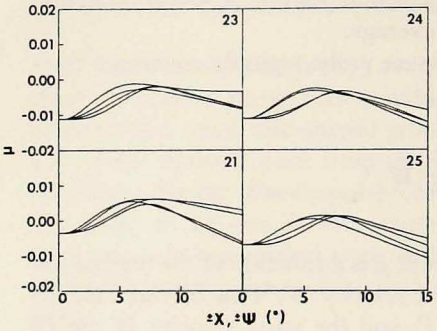

Figure 1. μ as a function of $\pm\chi$, $\psi = 0$, and $\pm\psi$, $\chi = 0$.

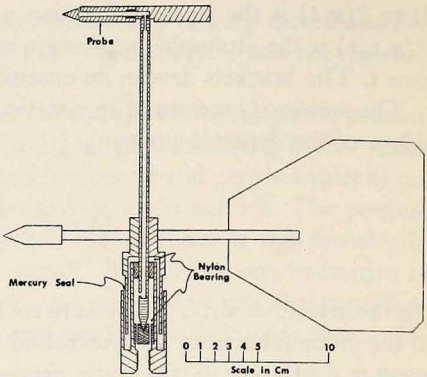

Figure 2. The vane assembly.

Thus,

$$\mu_0 = \mu(o,o),$$

$$\mu_1 = \chi_1 \frac{d}{d\chi}\mu(o,o) + \psi_1 \frac{d}{d\psi}\mu(o,o),$$

and

$$\mu'_1 = \chi'_1 \frac{\partial}{\partial\chi}\mu(o,o) + \psi'_1 \frac{d}{d\psi}\mu(o,o),$$

and μ_0, μ_1, and μ'_1 can be made to vanish by designing the probe so that $\mu(o,o) = o$, $\frac{d}{d\chi}\mu(o,o) = o$, and $\frac{d}{d\psi}\mu(o,o) = o$. While the present system design is capable of meeting these requirements exactly, they have been, in practice, only approximately met.

The basic probe design was suggested to the principal author by William Rainbird, following wind tunnel tests (by us) of disc- and wedge-shaped probes. A theoretical discussion of the pressure distribution along a cone has been presented by Laitone (1951). The probe is a 40° cone with a maximum diameter of 1.02 cm. Four 1-mm diameter holes are drilled into the face of the cone, nominally 1.19 cm from the tip of the cone along the face. The location of the holes is critical with respect to both μ_0 and μ_1. In order to insure an acceptable uniformity in the manufacture of the probes and to determine the optimum location of the probe holes, a drilling jig was constructed with a micrometer adjustment to control the hole location. A large number of blanks were machined, and several of these were drilled at various micrometer settings bracketing the optimum setting. The performance of the resulting probes was evaluated using the wind tunnel in the University of Miami's Department of Mechanical Engineering. A Pitot tube, made by United Sensors, with a reported pressure coefficient of .005, was used as a standard against which to compare the probes, and a Decker 360G differential pressure transducer was

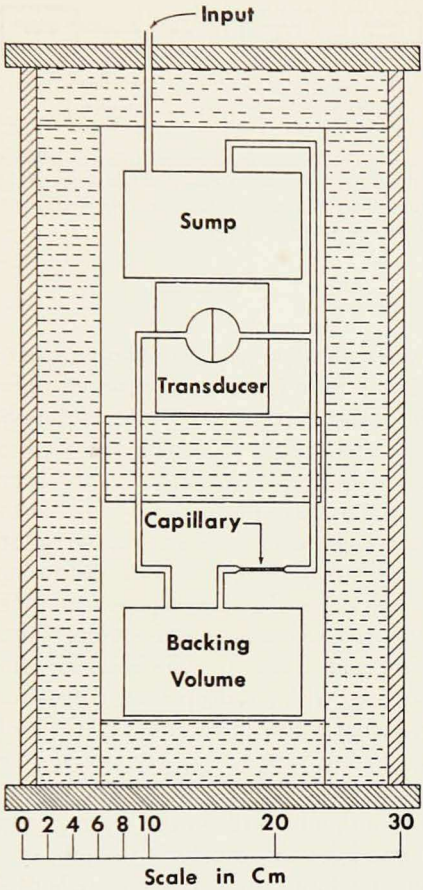

Figure 3. The microbarograph.

used to evaluate relevant pressure differences. The Pitot tube and the probe were alternately located at the same point in the test section and were compared by referencing them to a second fixed Pitot tube in the section. The angle of attack of the coned probe was varied between $\pm 20°$. On the basis of the evaluation of the initial set of probes, a second set was drilled, more closely bracketing the optimum. These probes were evaluated in the same fashion, and an optimum micrometer setting was determined. Ten blanks were drilled at the optimum setting and were individually evaluated. Four of these were chosen for use in the field experiment. The performance of these four probes, with angle of attack, is displayed in Figure 1 for a wind speed of 7.5 m/s. This performance is only slightly changed throughout the range 5–10 m/s. Typically, beyond $\pm 15°$ the pressure coefficient rapidly becomes more negative.

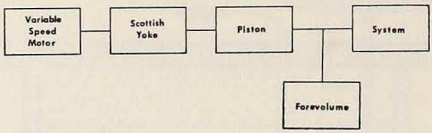

Figure 4. Pressure generator. The variable speed motor, a Zeromax Model JH1, was adjustable over two decades of frequency. The piston employed had a bore of 1.5 cm and a stroke of 3.8 cm. The forevolume was 82 liters and contained 6.5 Kg of steel wool. The volume was packed in vermiculite inside a 220-liter drum.

3. The vane

The dynamics of wave motions provide a natural limit to the vertical angle of attack experienced by a fixed horizontal probe, assuming that the flow does not separate from the water surface. The rule-of-thumb 1/7 slope at which waves are said to break corresponds to an angle of 8°, well within the acceptable range of the cone-shaped probe described in the previous section.

Horizontal angles of attack are not naturally limited to such a small range. As anyone who has watched a wind vane knows, swings of 30° or more are not untypical of winds in the range 5–10 m/s. In order to limit the effect of such swings on the horizontal angle of attack experienced by the probe, this probe was mounted on a vane, free to orient into the wind. The response of this vane has not been studied in detail; however, with wind speeds of 5 m/s and greater, the time constant associated with a sudden change of wind direction is of order .2 s. Thus, in the frequency range .5 to 5. rad/s, it is highly unlikely that the signal is contaminated by horizontal angles of attack exceeding the 15° limit. A diagram of the vane is provided in Figure 2. The vane employs a water-tight bearing with a mercury seal, which allows the bearing to be submerged without leaking water to the standpipe that conducts the pressure signal below.

While the vane assembly limits the horizontal angle of attack experienced by the probe and consequently reduces the noise resulting from the sensitivity of the pressure coefficient to angle of attack, this assembly is, itself, a source of system noise:

1) The swinging of the vane causes centrifugal pressures to be developed between the probe holes and the axis of the vane.

2) The upper nylon bearing provides a secondary path by which fluctuations of static or dynamic pressure can reach the top of the standpipe.

3) Motions of the mercury seal cause internal pressure fluctuations which can reach the top of the standpipe.

Centrifugal pressures associated with 1) are of order $1/2\rho\theta^2\omega^2r^2 \sim .1$ μbar, where ρ is the density of air, θ is a typical angular deviation of the probe azimuth from the mean, ω is a typical frequency, and r is the distance of the probe holes from the axis of the vane. Direct measurement of path resistances indicates that the resistance of the secondary path is approximately 150 times that

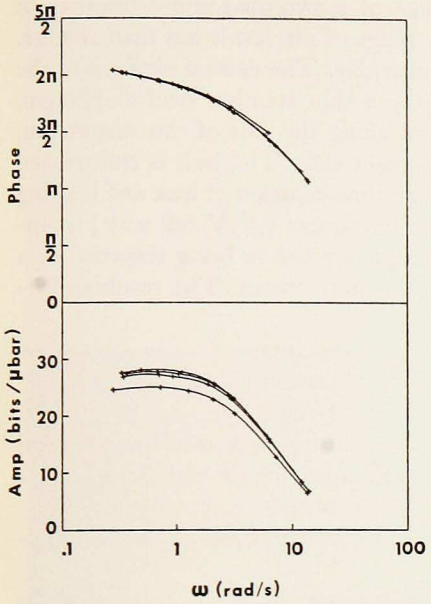

Figure 5. System response for the four instruments used in the field experiments.

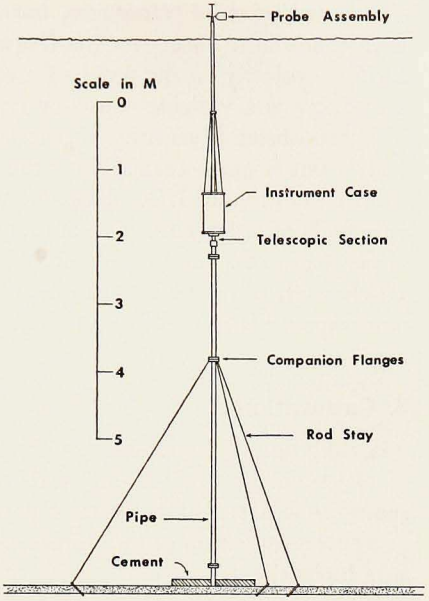

Figure 6. Field installation of the atmospheric pressure sensor.

of the primary path. The resulting dynamic pressure noise associated with 2) is of order .003 $(P_1 + P'_1)$, assuming an effective pressure coefficient for the secondary path of .5. Static pressure noise is probably much smaller because the static pressure signal carried by the secondary path is essentially identical with that carried by the primary path. The noise resulting from 3) appears to be associated with fluctuations in the orientation of the vane, and is largely wave-incoherent. Field tests with the primary path blocked indicate a corresponding noise level of less than .1 μbar.

4. The microbarograph

The pressure signal is carried from the vane assembly to a subsurface microbarograph by a 3-m vertical standpipe. The standpipe is constructed of two lengths of coaxial tubing, a structural length of 5-cm O.D. aluminum tubing, and a length of 6-mm O.D. stainless steel tubing to conduct the signal. A small sump is located at the base of the standpipe to collect any water which might be introduced into the system from above.

The microbarograph is diagramed in Figure 3. The instrument, modeled after an instrument developed by the National Bureau of Standards (see Priestley, 1965), consists of a sump forevolume, backing volume, and leak insulated with 2 inches of polyurethane foam. The transducer, a Decker 360G

differential pressure transducer, has a range of ± 250 μbar and a linearity of 2%. Transducer noise over the frequency range of interest is less than .1 μbar. Drift is typically on the order of several μbar/day. The central element of the transducer is a variable capacitor employing a thin stainless steel diaphragm. The transducer is sensitive to accelerations along the axis of this diaphragm, which axis is made coaxial with the instrument case. The leak is constructed from 1 m of .7 mm I.D. copper tubing. The time constant of leak and backing volume is of order 10 s. The output of the transducer (± 5V full scale) is amplified (gain of 4) and rolled off at high frequency before being recorded by a 16-channel, computer-compatible, data-acquisition system. The resulting system response is shown in Section 5.

5. Calibration

Calibration of a microbarograph system may be approached in several ways:

1) Comparison of the output of the system with that of "standard" in response to a (series of) pressure input(s).

2) Determination of the response of the system to a (series of) known pressure input(s).

The calibration of the present system was accomplished by combining the two approaches. A sine wave pressure generator was constructed, as diagramed in Figure 4. To help insure an isothermal change of pressure (the transition from adiabatic to isothermal change of pressure occurs in the frequency range of interest), the generator forevolume was packed with steel wool, the heat capacity of which was sufficient to hold the proportional change of temperature of the forevolume to 1% of the proportional change of pressure. The forevolume was 90 times larger than the sump forevolume in the microbarograph, minimizing the effect of the load on the pressure signal generated. The pressure signal calculated from the piston displacement and the generator forevolume, assuming an isothermal change of pressure, was compared at various frequencies with the signal monitored by a Decker 360G transducer with one side open to the atmosphere. Amplitudes and phases were consistent within experimental error at frequencies below 2 rad/s (frequencies below .4 rad/s were not investigated), with the observed amplitude ~ 97% of calculated at 2 rad/s, 94% of calculated at 4 rad/s, and 77% of calculated at 10 rad/s. The observed signal lagged the calculated by .1 at 2 rad/s, .2 at 4 rad/s, and .4 at 10 rad/s. The loss of amplitude and attendant phase lag at frequencies above 2 rad/s are associated with generator plumbing and with the (imperfectly known) response of the Decker standard. The instrument calibrations shown in Figure 5 (and employed in the analysis of the BOA field experiments) assume this response to be "instantaneous." To the extent that this assumption fails, the calibrations may contain a systematic error as large as the above discrepancies.

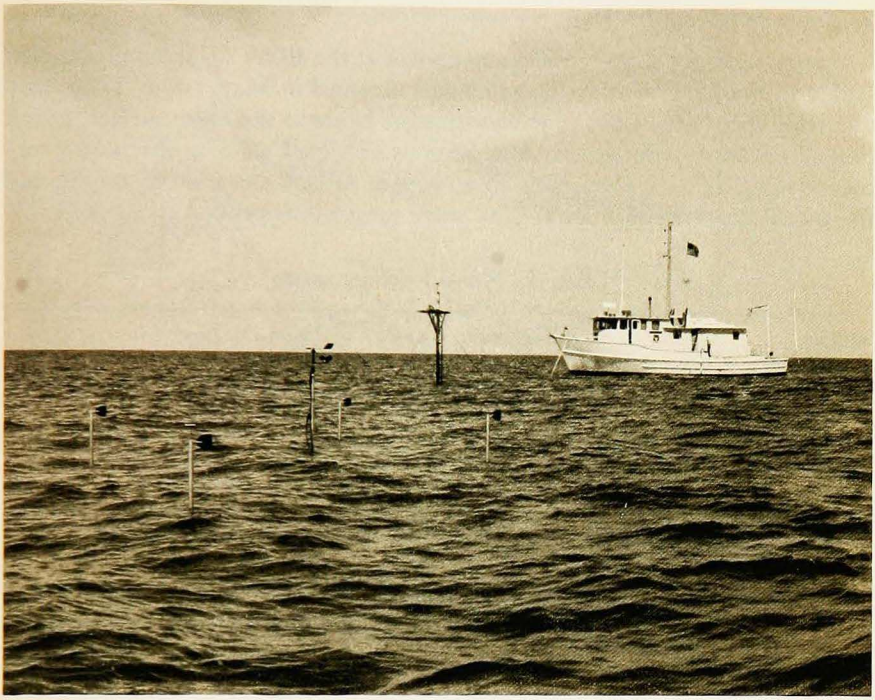

Figure 7. Field configuration. Vessel shown is the L. F. R. BELLOWS.

6. Field installation

The field installation of an atmospheric pressure sensor at the BOA site is pictured in Figure 6. The instrument is supported from below by a guyed stand of simple construction. This stand holds the horizontal position of the probe steady to within 5 cm. Vertical adjustment of the stand allows the probe to be placed anywhere within 2 m of the mean surface. Installation of the instrument by a pair of SCUBA divers is possible in winds up to 7 m/s. The probe assemblies may be placed on or removed from the standpipes in winds up to 10 m/s from a small boat (we use a Boston Whaler).

A photograph of four instruments in place at the BOA site is shown in Figure 7. Not shown are four Snodgrass Mark X wave recorders mounted on unguyed stands. A cup anemometer is mounted on the central wave recorder stand. Cables run from the instruments and from a tide gauge and cup anemometer on the tower shown in the photograph to a laboratory vessel located 125 m to the west of the array. Aboard ship, the resulting signals are recorded with a 16-channel, computer-compatible, data-acquisition system (Radiation Inc., Model 5015).

7. Noise level

System noise for a typical field experiment at the BOA site is summarized in Table I. Noise estimates are based on data obtained in May, 1970. They apply to a wind speed of 7.5 m/s (5 m elevation), 1 m above the mean surface, which produces a wave-induced atmospheric pressure signal of ~ 4 μbar and a turbulent signal of ~ 4 μbar. The mean square surface elevation is .01 m^2, and the mean square slope is .002. The wave spectrum is peaked at 2.1 rad/s.

Table I. Noise level estimates.

Source	Magnitude	Remarks
wave-coherent dynamic pressures	$\sim \mu_0 P_1 \sim .04$ μbar	error frequency dependent
wave-incoherent dynamic pressures	$\sim \mu_0 P_1' \sim .04$ μbar	peaked at low frequency
wave-coherent fluctuations in angle of attack	$\sim \frac{1}{2} \mu_1 \varrho W_0^2$	small because of probe symmetry
	$\sim \frac{1}{2} \mu_2 \varrho W_0^2 \sim .25$ μbar	based on $<\psi^2> \sim .002$. Produce wave-incoherent contribution because of frequency doubling. Implied peak in spectrum not apparent
wave-incoherent fluctuations in angle of attack	$\sim \frac{1}{2} \mu_1' \varrho W_0^2$	small because of probe symmetry
	$\sim \frac{1}{2} \mu_2' \varrho W_0^2 < .25$ μbar	assuming $<\chi'^2> < .002$
centrifugal pressures in system plumbing	$< .1$ μbar	
secondary input through mercury seal	$\sim .003 (P_1 + P_1')$	
internal pressures associated with motion of mercury seal	$< .1$ μbar	largely wave-incoherent
thermodynamic fluctuations associated with temperature sensitivity of standpipe and microbarograph	$< .1$ μbar	
mechanical motions of standpipe and microbarograph	$< .1$ μbar	includes dynamic pressures generated by probe translations
electronics	$\sim .1$ μbar	
digitization error	$\sim .03$ μbar	

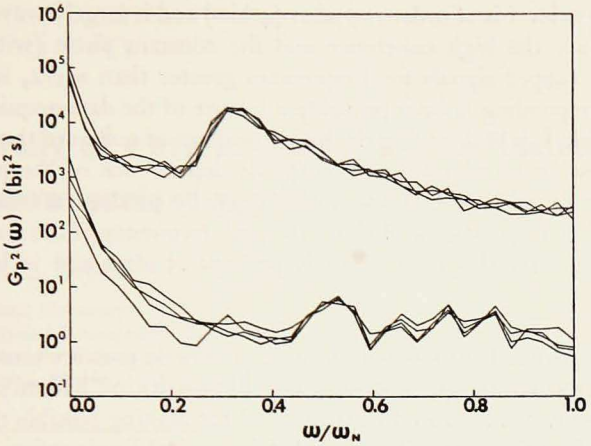

Figure 8. Noise determination. The upper curves show a typical spectrum with the atmospheric pressure sensors operating normally. The lower curves show the corresponding noise spectrum (not including vane- or probe-generated noise) with the standpipe capped. The peak at $\omega/\omega_N \sim .3$ is wave-induced. The Nyquist frequency ω_N is 6.85 rad/s.

Special comment is warranted with respect to the first entry in the table. In the potential theory limit, the first-order pressure is of order

$$P_1 \sim \frac{\varrho}{k}(\boldsymbol{k}\cdot\boldsymbol{W}-\omega)^2\zeta_1,$$

where ζ_1 is the first-order surface elevation, $\boldsymbol{k}$ is the propagation vector of a given wave component, and ω is its radial frequency. The first-order dynamic pressure is of order

$$D_1 \sim \frac{\varrho}{k}\boldsymbol{k}\cdot\boldsymbol{W}(\boldsymbol{k}\cdot\boldsymbol{W}-\omega)\zeta_1.$$

Thus D_1/P_1 is of order

$$\frac{\boldsymbol{k}\cdot\boldsymbol{W}}{(\boldsymbol{k}\cdot\boldsymbol{W}-\omega)}.$$

To the extent that potential theory predicts this ratio properly, it is clear that on the low-frequency face of the spectrum the relative error can be very large indeed. Note, however, that here both P_1 and D_1 are vanishingly small, so that the absolute error is bounded. At higher frequencies, the error approaches the level shown in the table.

An estimate of the combined effect of the last four entries in Table I (excluding dynamic pressures generated by probe translations) is shown in Figure 8. Spectra are displayed for: 1) normal operation of the microbarographs and 2) operation with the standpipes capped (vanes and probes removed). The corre-

sponding noise level is of order .15 μbar (4 bits) and is largely wave-incoherent. Not shown are the high coherence and the constant phase (with frequency) between the capped signals for frequencies greater than $\omega_N/2$, which suggest that the corresponding noise is probably a feature of the data-acquisition system.

From Table I, it is clear that the largest sources of noise are the second-order dynamic pressure terms associated with the dependence of the pressure coefficient on angle of attack. These terms typically produce a wave-incoherent contribution at frequencies well above the peak frequency of the wave spectrum. The resulting overall system noise is perhaps .5 μbar and is largely wave-incoherent.

Acknowledgments. Development of the atmospheric pressure sensor was begun while the principal author was with the University of Miami's Institute of Marine Science. Dr. Samuel Lee is thanked for making possible the use of the wind tunnel facilities of the University's Mechanical Engineering Department. Valuable discussions with O. Shemdin are acknowledged. Support for the project has been provided by Office of Naval Research Grants N00014-67-A-0386-0001 and NONR 4008(02).

REFERENCES

Dobson, F. W.
1971. Measurements of Atmospheric Pressure on Wind-generated Sea Waves, J. Fluid Mech., *48*: pp. 91–127.

Elliott, J. A.
1972. Microscale Pressure Fluctuations Near Waves Being Generated by Wind, J. Fluid Mech., *54*: pp. 427–448.

Laitone, E. V.
1951. Experimental Measurement of Incompressible Flow Along a Cylinder with a Conical Nose, J. Appl. Phys., *22*(1): pp. 63–64.

Longuett-Higgins, M. S., D. E. Cartwright, and N. D. Smith
1963. Observations of the Directional Spectrum of Sea Waves Using the Motions of a Floating Buoy, in Ocean Wave Spectra, Prentice-Hall, pp. 111–136.

Priestley, J. T.
1965. Correlation Studies of Pressure Fluctuations on the Ground beneath a Turbulent Boundary Layer, U.S. Nat. Bur. Standards Report 8942, 92 pp.

Shemdin, O. H.
1969. Instantaneous Velocity and Pressure Measurements above Propagating Waves, U. Florida Dept. Coast and Ocean. Engineering Report 4, 105 pp.

Shemdin, O. H., and E. Y. Hsu
1966. The Dynamics of Wind in the Vicinity of Progressive Water Waves, J. Fluid Mech., *30*: pp. 403–416.